## EDGE ARTICLE

Check for updates

# An effective design strategy for thermally activated delayed fluorescence emitters with aggregation-induced emission to enable sky-blue OLEDs that achieve an EQE of nearly 30%†

Hui Dai,[a] Yaohui Liang,[a] Xiang Long,[a] Tianyi Tang,[a] Haozhi Xie,[a] Zhiwei Ma,[a] Gaoyu Li,[a] Zhan Yang, *[b] Juan Zhao *[b] and Zhenguo Chi *[ab]

Pure organic thermally activated delayed fluorescence (TADF) materials hold great promise for efficient organic light-emitting diodes (OLEDs), yet developing high-performance blue TADF materials that integrate short delayed lifetime with aggregation-induced emission (AIE) properties remains a significant challenge. In this study, we developed three highly-efficient blue TADF emitters (32clCBP, 32clCXT and 32PclCXT) featuring AIE character by integrating rigid π-extended donors with different acceptors. Notably, the doped 32PclCXT film achieved an exceptionally high photoluminescence quantum efficiency of up to 99% and a short delayed lifetime of 1.4 μs. Furthermore, the fabricated OLEDs based on 32PclCXT exhibited an impressive external quantum efficiency of 29.9% in the sky-blue region, along with low roll-off at high luminance. Therefore, this work establishes a new strategy for developing high-efficiency blue TADF materials and devices.

## Introduction

Pure organic thermally activated delayed fluorescence (TADF) materials have garnered widespread attention from both academia and industry due to their ability to harvest both singlet and triplet excitons through reverse intersystem crossing (RISC), along with their merits of low cost and environmental friendliness,[1–4] thus they are considered as third generation emitters for organic light-emitting diode (OLED) application.[5,6] A common approach to designing TADF molecules involves highly-twisted molecular structures with electron donor (D) and electron acceptor (A) groups, which help achieve a small energy difference ($\Delta E_{ST}$) between the lowest excited singlet state ($S_1$) and triplet state ($T_1$) by separating the highest occupied molecular orbital (HOMO) and the lowest unoccupied molecular orbital (LUMO), thereby facilitating a fast RISC process.[7] Consequently, a wide range of high-performance OLEDs based on TADF emitters, spanning from the ultraviolet to near-infrared region, have been developed over the past decade.[8–11]

Despite that, highly efficient blue TADF materials remain limited, and the development of efficient blue TADF materials is of great significance due to the critical importance of blue OLEDs for commercial applications.

Due to its rigidity and moderate electron donating ability, carbazole has been widely employed as an electron donor group to develop blue TADF materials.[12–15] Nevertheless, a significant portion of these TADF materials suffer from the aggregation-caused quenching (ACQ) effect, resulting from π–π stacking interactions between molecules,[16–18] which significantly hinders their practical applications. Interestingly, indolocarbazole derivatives have emerged as alternative electron donor groups for efficient blue TADF emitters, offering high molecular rigidity and substantial steric hindrance, thereby mitigating the ACQ effect.[19,20] For example, Xi and colleagues[19] designed blue TADF molecules with aggregation-induced emission (AIE) properties using indolocarbazole derivatives, achieving an external quantum efficiency (EQE) of 20.8% for blue OLEDs. Then, Yao *et al.*[21] obtained efficient blue emitters with AIE and TADF properties by locking the skeleton of indolocarbazole derivatives. Despite these advancements, there are still no reports regarding TADF emitters based on indolocarbazole derivatives affording blue OLEDs with EQEs up to 30%, the upper limit for common bottom-emitting OLEDs.

In this context, we report three efficient blue emitters with AIE and TADF properties (Fig. 1) based on an indolocarbazole derivative (5,12-dihydro-12-phenylindolo[3,2-*a*]carbazole), phenyl(4-(12-phenylindolo[3,2-*a*]carbazol-5(12*H*)-yl)phenyl)

*[a]PCFM Lab, GD HPPC Lab, Guangdong Engineering Technology Research Center for High-performance Organic and Polymer Photoelectric Functional Films, State Key Laboratory of Optoelectronic Material and Technologies, School of Chemistry, Sun Yat-sen University, Guangzhou 510275, PR China. E-mail: chizhg@mail.sysu.edu.cn*

*[b]School of Environmental and Chemical Engineering, Wuyi University, Jiangmen 529020, China. E-mail: zhaoj95@mail.sysu.edu.cn; yangzhan.asd@foxmail.com*
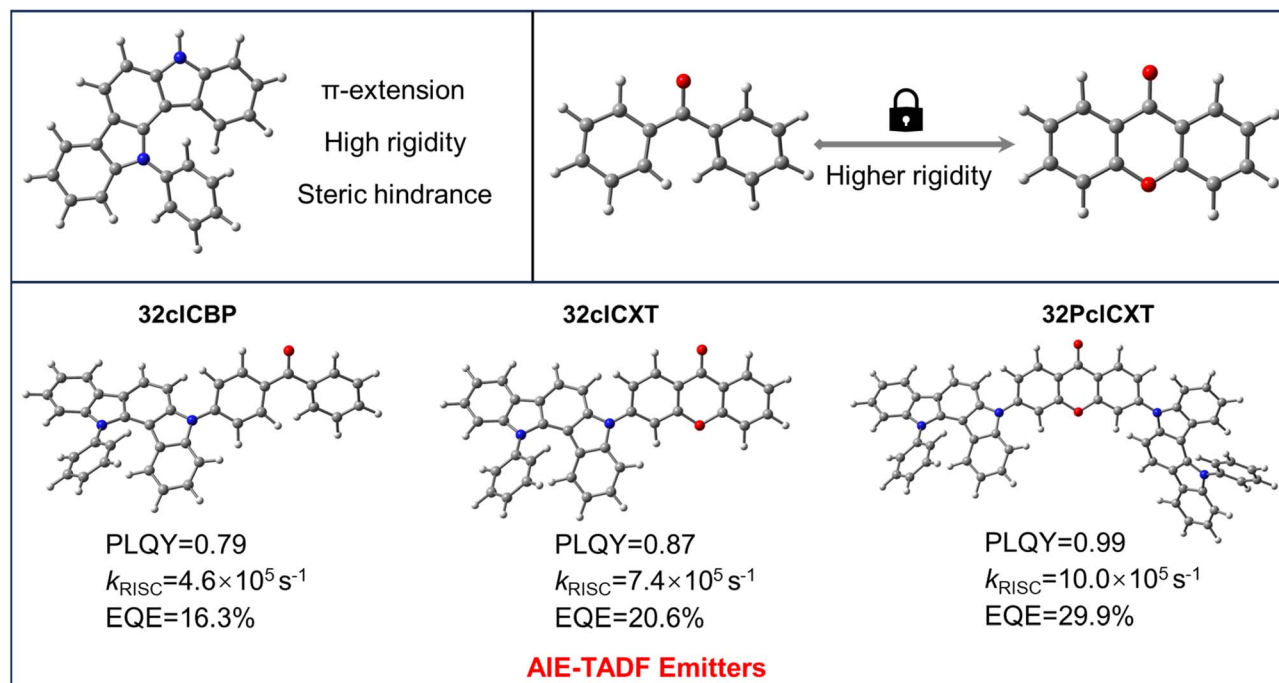
**Fig. 1** Design strategy of AIE-TADF materials.

methanone (32clCBP), 3-(12-phenylindolo[3,2-*a*]carbazol-5(12*H*)-yl)-9*H*-xanthen-9-one (32clCXT), and 3,6-bis(12-phenyl-indolo[3,2-*a*]carbazol-5(12*H*)-yl)-9*H*-xanthen-9-one (32PclCXT). The benzophenone (BP) and xanthenone (XT) acceptor units were connected with the 5,12-dihydro-12-phenylindolo[3,2-*a*] carbazole donor directly to obtain molecules with D–A/D–A–D structures. Compared to the BP group, the XT unit exhibits greater planarity and rigidity, which help to reduce structural relaxation of excited states and enhance photoluminescence quantum yields (PLQYs) in the aggregated state.[22–24] Consequently, the PLQYs of the resulting compounds (32clCXT and 32PclCXT) are improved compared to that of 32clCBP, leading to enhanced electroluminescence (EL) performance. The two novel luminogens based on the XT acceptor demonstrate remarkable AIE-TADF properties, characterized by high PLQYs, small $\Delta E_{ST}$ values, and short delayed fluorescence lifetimes. The doped OLEDs utilizing 32PclCXT exhibit sky-blue emission with outstanding EL performance, achieving a maximum EQE (EQE$_{max}$) of 29.9% with low efficiency roll-off at a high luminance of 1000 cd m$^{-2}$. This work presents a novel and effective strategy for constructing high-efficiency blue TADF materials and devices.

## Results and discussion

### Synthesis and characterization

The synthetic procedures for the three target compounds are provided in Scheme S1 (ESI†) and structural characterization studies are conducted by $^1$H and $^{13}$C nuclear magnetic resonance (NMR) spectroscopy and high-resolution mass spectroscopy (Fig. S1–S9, ESI†). As depicted in Fig. S11a (ESI†), all the compounds possess a high decomposition temperature ($T_d$,

corresponding to 5% weight loss) of 379 °C, 413 °C and 544 °C for 32clCBP, 32clCXT and 32PclCXT, respectively, indicating their excellent thermal stability. 32clCBP, 32clCXT and 32PclCXT exhibit a glass transition temperature ($T_g$) of 100 °C, 142 °C and 233 °C, respectively (Fig. S11b, ESI†), which is beneficial for obtaining a stable film morphology during device operation. According to the energy gaps obtained from absorption onsets (Fig. S12a, ESI†) and the corresponding onset voltages of cyclic voltammetry curves (Fig. S12b, ESI†), the HOMO/LUMO energy levels are measured to be −5.36 eV/−2.43 eV for 32clCBP, −5.39 eV/−2.53 eV for 32clCXT and −5.38 eV/−2.63 eV for 32PclCXT, respectively (Table S1, ESI†). XT exhibits stronger electron-withdrawing ability than BP and therefore XT-based TADF emitters have deeper LUMO levels.

### Theoretical calculations

To shed light on the geometrical structures and frontier molecular orbital (FMO) distributions, density functional theory (DFT) calculations were performed using the Gaussian program at the B3LYP/6-31g(d,p) basis set for the three compounds. As shown in Fig. S13,† the emitters show twisted structures, with the donors and acceptors forming large torsion angles of 50.31–51.89°. The LUMOs are primarily located on the XT or BP acceptor units, whereas the HOMOs are distributed on the 5,12-dihydro-12-phenylindolo[3,2-*a*]carbazole donor, extending slightly to adjacent phenyl rings of the acceptors (Fig. S14†). Furthermore, time-dependent DFT with the PBE0 functional at the same basis set was employed to assess the energy levels of the excited states and perform natural transition orbital (NTO) analyses. The calculated $\Delta E_{ST}$ values for 32clCBP, 32clCXT, and 32PclCXT were found to be 0.36 eV, 0.30 eV and 0.21 eV, respectively. Further analysis of the NTO

pairs reveals that several triplet states exist below the $S_1$ energy level (Fig. 2 and S15–S17, ESI†). For 32clCBP and 32clCXT, the $T_2$ state exhibits significant locally-excited ($^3LE$) characteristics, with small energy gaps of 0.21 eV and 0.19 eV, respectively, between $S_1$ and $T_2$. Interestingly, 32PclCXT shows degenerate excited states ($T_1/T_2$) due to its symmetrical structure, and $T_3$ demonstrates a significant LE ($^3LE$) characteristic with a minimal energy gap of 0.07 eV between the $^3CT$ and $^3LE$. The $^3LE$ state facilitates efficient coupling between the $^3CT$ and the $^1CT$, potentially leading to enhanced RISC and superior OLED performance.[9]

## Photophysical properties

To investigate the photophysical properties of the three compounds, their ultraviolet-visible (UV-vis) absorption and photoluminescence (PL) spectra were measured in dilute toluene solutions ($1 \times 10^{-5}$ mol L$^{-1}$), as shown in Fig. 3a–c. All three emitters exhibit strong absorption around 300 nm, corresponding to delocalized $\pi$–$\pi^*$ transition of the 5,12-dihydro-12-phenylindolo[3,2-$a$] carbazole core. Additionally, a broad and weaker absorption peak is observed from 330 to 400 nm, due to intramolecular charge transfer (ICT) from the donor to the acceptor units. The PL spectra of 32clCBP, 32clCXT and 32PclCXT display structureless emissions with peaks at 470 nm, 476 nm, and 488 nm, respectively. To further explore their excited-state properties, solvatochromic experiments were conducted, revealing a significant dependence of the PL spectra on solvent polarity (Fig. S18, ESI†). The Stokes shifts with increasing solvent polarity confirmed the typical ICT characteristics of the compounds. Moreover, the $\Delta E_{ST}$ values were determined *via* phosphorescence spectra to be 0.21 eV for 32clCBP, 0.15 eV for 32clCXT, and 0.14 eV for 32PclCXT (Fig. 3a–c), indicating their TADF properties. Interestingly, the phosphorescence spectra of the three compounds exhibit fine vibrational structures, indicative of a locally-excited triplet state ($^3LE$). Additionally, the phosphorescence spectra of the emitters were also measured in highly polar solvent (Dimethyl sulfoxide (DMSO)). As shown in Fig. S19,† only 32PclCXT displays an

obvious structureless peak ($^3CT$), which is 0.1 eV lower than that of the $^3LE$ state, aligning with the theoretical calculation results. The presence of the $^3LE$ state with an appropriate energy level in all three compounds ensures an efficient RISC process, thereby enhancing their TADF performance.

Surprisingly, the PL emission intensities of the three emitters significantly increase with the formation of aggregates upon the addition of a large amount of water into DMSO solutions (Fig. 3d–f and S20, ESI†). Concurrently, their fluorescence lifetimes become notably longer, displaying clear delayed components, which indicates the presence of aggregation-induced delayed fluorescence (Fig. S21, ESI†).[25] In the solution state, vigorous intramolecular motions and the presence of oxygen can nonradiatively deactivate the excited state and hinder both the ISC and RISC processes, leading to weak emission and the absence of delayed fluorescence.[26] These results demonstrate that the introduction of indolocarbazole derivatives enables emitters to possess both AIE and TADF properties.

Furthermore, their doped films (20 wt% in the bis[2-(diphenylphosphino)phenyl]ether oxide (DPEPO) host) demonstrate strong PL intensities, with emission peaks at 489 nm, 492 nm, and 508 nm for 32clCBP, 32clCXT, and 32PclCXT (Fig. S22†), respectively. These peaks are significantly red-shifted compared to their PL spectra in toluene, which can be attributed to the relatively high polarity of DPEPO and potential molecular interactions between the host and the emitters.[5] Meanwhile, the PLQYs of 32clCBP, 32clCXT, and 32PclCXT in doped films were measured, reaching 79%, 87%, and 99%, respectively, under ambient conditions (Fig. 4b). Notably, the PLQYs of the XT derivatives are considerably higher than those of the BP derivative. The PL decay curves in doped films exhibit double-exponential behavior, showing both a nanosecond prompt decay and a microsecond delayed decay (Fig. 4a), with delayed lifetimes of 2.8 μs (32clCBP), 1.8 μs (32clCXT), and 1.4 μs (32PclCXT). Furthermore, the proportion of the delayed components increases with the temperature rising from 77 K to 300 K (Fig. S23, ESI†), providing further evidence for the TADF feature of the three compounds. The TADF process is additionally supported by oxygen-sensitive PL spectra (Fig. S24, ESI†). Based on their fluorescence and phosphorescence spectra (Fig. S22, ESI†), the doped films exhibit tiny $\Delta E_{ST}$ values of 0.26 eV, 0.04 eV, and 0.03 eV for 32clCBP, 32clCXT, and 32PclCXT, respectively. These small $\Delta E_{ST}$ values promote the occurrence of TADF and align well with our experimental observations. Subsequently, kinetic parameters based on the PLQYs and lifetimes were analyzed. As displayed in Fig. 4c and Table 1, the reverse intersystem crossing rate constants ($k_{RISC}$) for 32clCXT and 32PclCXT are $7.4 \times 10^5$ s$^{-1}$ and $1.0 \times 10^6$ s$^{-1}$, respectively, which are significantly higher than that of 32clCBP ($4.6 \times 10^5$ s$^{-1}$), indicating a faster TADF process in XT derivatives. Furthermore, the non-radiative rate constants ($k_{nr}$) for 32clCXT ($4.6 \times 10^5$ s$^{-1}$) and 32PclCXT ($3.4 \times 10^5$ s$^{-1}$) are notably lower compared to that of 32clCBP ($9.6 \times 10^5$ s$^{-1}$), suggesting excellent TADF performance and efficient exciton utilization of the XT derivatives. These results clearly



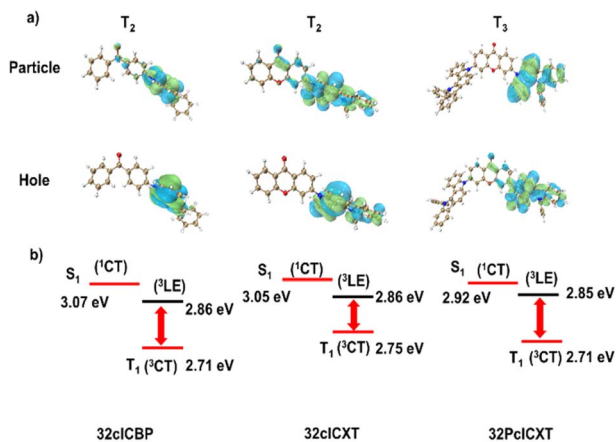**Fig. 2** (a) Natural transition orbitals, and (b) energy level alignments of the $^1CT$, $^3CT$, and $^3LE$ states of 32clCBP, 32clCXT and 32PclCXT.
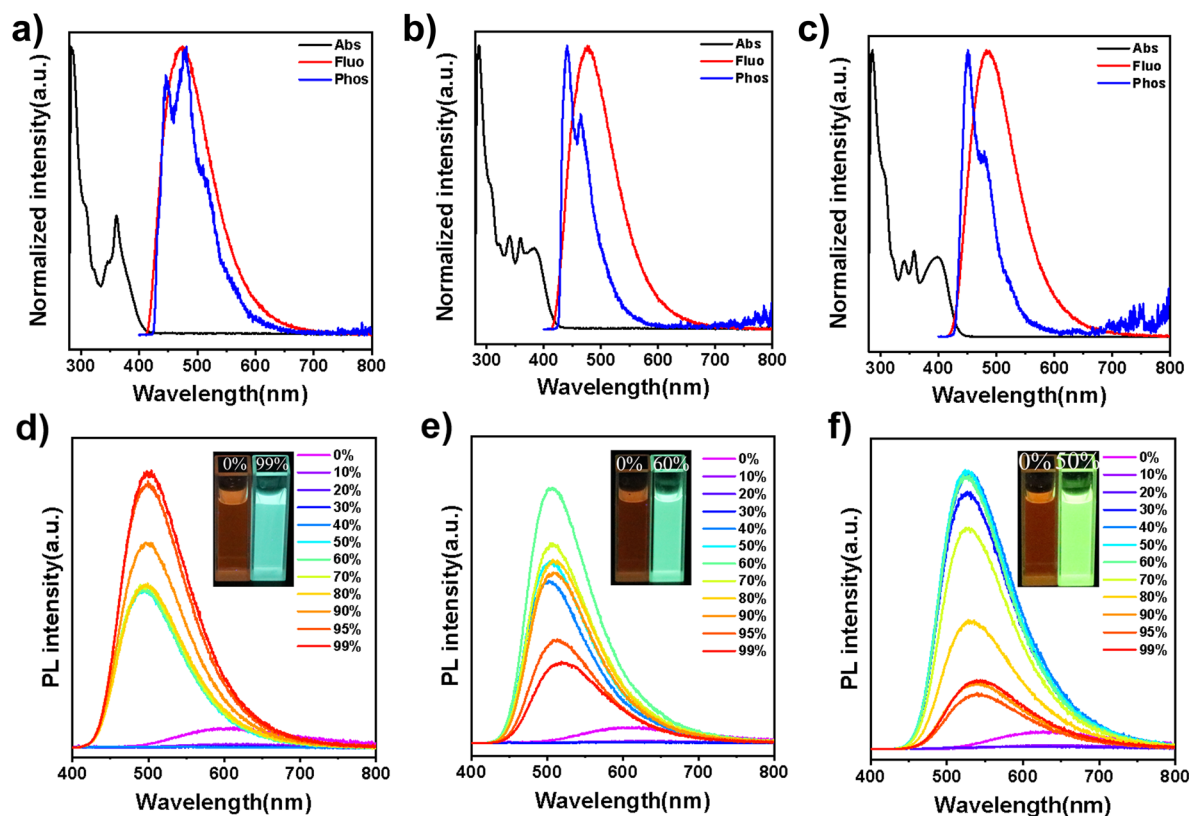
**Fig. 3** UV-vis absorption and fluorescence at 300 K, and phosphorescence spectra at 77 K in toluene solutions (concentration: $10^{-5}$ M) of (a) 32clCBP, (b) 32clCXT, and (c) 32PclCXT. Photoluminescence spectra of (d) 32clCBP, (e) 32clC-XT, and (f) 32PclCXT in $H_2O$/DMSO mixtures with different water contents (concentration: $10^{-5}$ M).
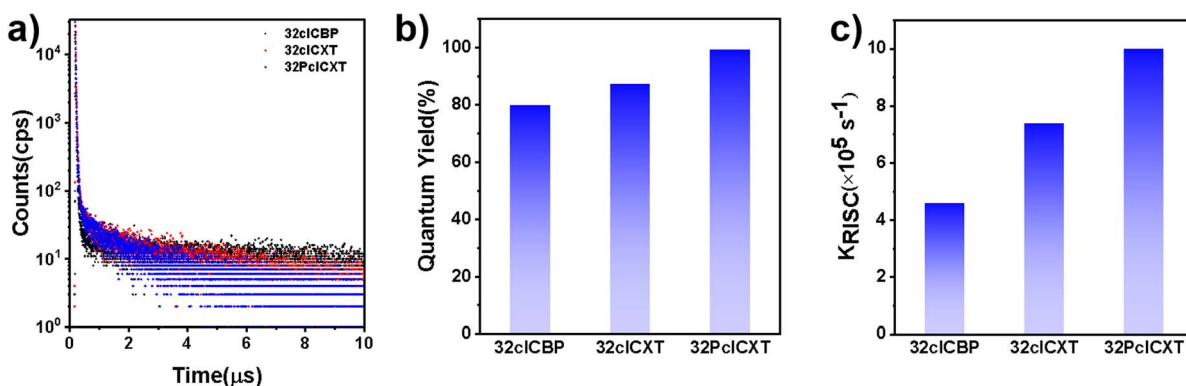


**Fig. 4** (a) Transient PL decay curves, (b) PLQYs, and (c) $k_{RISC}$ of doped 32clCBP, 32clCXT and 32PclCXT films (20 wt% in DPEPO).

**Table 1** Summary of photophysical properties of 32clCBP, 32clCXT and 32PclCXT in doped films

| Molecule | $\lambda_{max}{}^a$ [nm] | $\tau_p{}^b$ [ns] | $\tau_d{}^c$ [μs] | PLQY$^d$ [%] | $\Phi_{PF}{}^e$ [%] | $\Phi_{DF}{}^f$ [%] | $k_r{}^g$ [$10^6$ s$^{-1}$] | $k_{nr}{}^h$ [$10^5$ s$^{-1}$] | $k_{ISC}{}^i$ [$10^7$ s$^{-1}$] | $k_{RISC}{}^j$ [$10^5$ s$^{-1}$] |
|---|---|---|---|---|---|---|---|---|---|---|
| 32clCBP | 490 | 16.7 | 2.8 | 80 | 62.7 | 17.1 | 3.7 | 9.6 | 1.3 | 4.6 |
| 32clCXT | 492 | 21.4 | 1.8 | 87 | 66.1 | 21.0 | 3.1 | 4.6 | 1.1 | 7.4 |
| 32PclCXT | 506 | 19.9 | 1.4 | 99 | 72.3 | 26.8 | 3.6 | 3.4 | 1.3 | 10.0 |

$^a$ PL emission peak. $^b$ Prompt lifetime. $^c$ Delayed lifetime. $^d$ Photoluminescence quantum yield measured under air. $^e$ Absolute quantum yield of prompt fluorescence. $^f$ Absolute quantum yield of delayed fluorescence. $^g$ Rate constant of radiative decay. $^h$ Rate constant of nonradiative decay. $^i$ Rate constant of intersystem crossing. $^j$ Rate constant of reverse intersystem crossing.
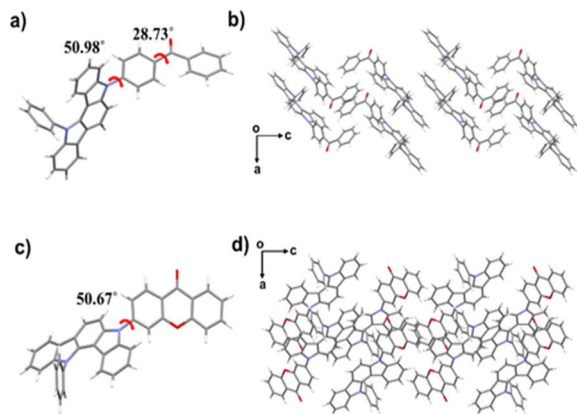
Fig. 5 Single-crystal structures of (a) 32clCBP and (c) 32clCXT. Packing modes of (b) 32clCBP and (d) 32clCXT in single crystals.

demonstrate that the TADF performance can be significantly enhanced by introducing the XT group instead of the BP group.

To gain further insights into the AIE-TADF mechanism of the three compounds, detailed crystal structure analyses were conducted. Single crystals of 32clCBP and 32clCXT were successfully obtained by solvent evaporation from mixed solvents, however, single crystals of 32PclCXT could not be isolated. As depicted in Fig. 5, both 32clCBP and 32clCXT exhibit twisted molecular conformations, which effectively restrict close packing and weaken π–π interactions between adjacent molecules, thereby imparting AIE-TADF properties to all emitters.

### Electroluminescence performance

In light of their excellent PL efficiencies and prominent delayed fluorescence in doped films, a series of doped OLEDs based on the three emitters were fabricated using vacuum deposition

technology. The device structure is illustrated in Fig. 6a: indium tin oxide (ITO)/hexaazatriphenylene hexacabonitrile (HATCN, 5 nm)/1,10-bis(di-4-tolylaminophenyl) cyclohexane (TAPC, 30 nm)/tris[4-(carbazol-9-yl)phenyl]amine (TCTA, 5 nm)/1,3-di(carbazol-9-yl)benzene (mCP, 5 nm)/emitting layer (EML, 20 nm)/1,3,5-tris(1-phenyl-1*H*-benzimidazol-2-yl)benzene (TPBi, 50 nm)/lithium fluoride (LiF, 1 nm)/Al (100 nm). The EMLs consisted of the DPEPO host with different concentrations of the TADF emitters, with HATCN and LiF serving as hole and electron injection layers, respectively. TAPC and TPBi functioned as hole and electron transport layers, respectively, while TCTA and mCP acted as electron blocking layers. Non-doped devices were also fabricated (Fig. S25 and Table S3, ESI†) while the device performances could be improved with further device optimizations in such as EML thickness and appropriate choice of organic functional layers. Gladly, the doped OLEDs presented excellent device performances, which are summarized in Table 2. All devices exhibited low turn-on voltages ranging from 2.8 V to 3.3 eV, emitting intense blue or sky-blue light. Notably, the driving voltage decreased with increasing doping concentration, indicating enhanced electron transport in the emitting layer (Table 2). The EL spectra showed slight redshifts as the doping concentration increases (Fig. S26–S28,† Table 2), attributed to exciton rearrangement from molecular aggregation.[11] At a doping concentration of 20 wt%, the emitters demonstrated optimal EL efficiencies. As shown in Fig. 6b, the EL spectral wavelengths for the doped devices peaked at 478 nm, 484 nm, and 500 nm for 32clCBP, 32clCXT, and 32PclCXT, respectively. The doped 32clCBP device achieved a maximum current efficiency ($CE_{max}$) of 35.5 cd A$^{-1}$, maximum power efficiency ($PE_{max}$) of 34.3 lm W$^{-1}$, and $EQE_{max}$ of 16.3%. In comparison, the doped 32clCXT device showed higher EL efficiencies with a $CE_{max}$ of 50.8 cd A$^{-1}$, $PE_{max}$ of 54.3 lm W$^{-1}$,
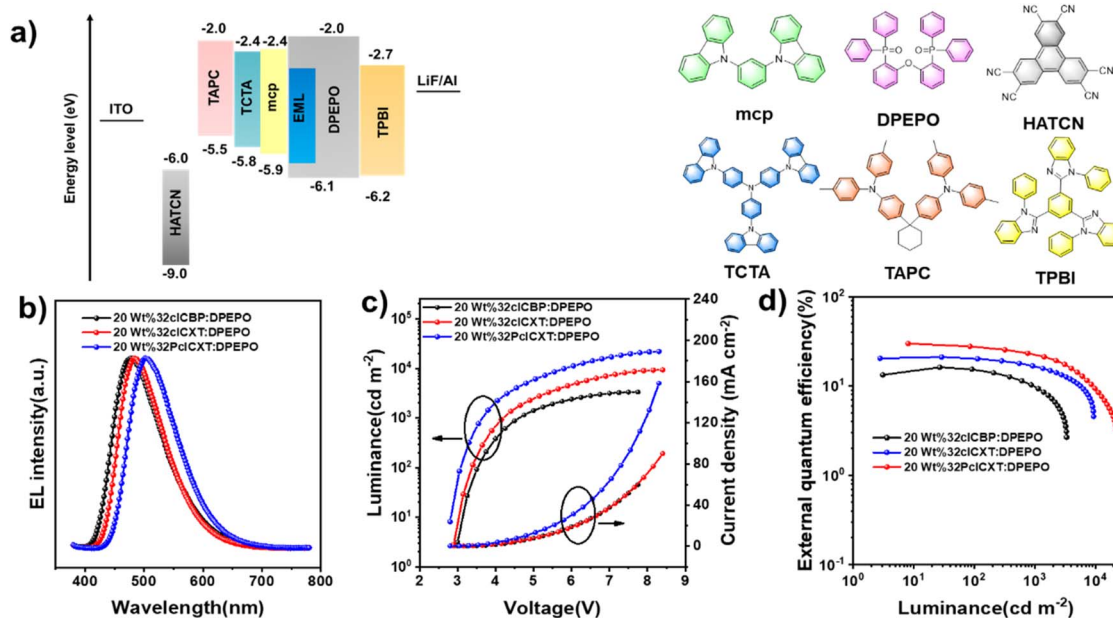


Fig. 6 (a) Device structure and chemical structures of organic functional layers. (b) EL spectra, (c) luminance–voltage–current density, and (d) external quantum efficiency–luminance curves of the OLEDs based on 32clCBP, 32clCXT and 32PclCXT.

**Table 2** EL performances of the doped OLEDs based on 32clCBP, 32clCXT and 32PclCXT

| EML | $\lambda_{EL}$ [nm] | $V_{on}$ [V] | $L_{max}$ [cd m$^{-2}$] | $CE_{max}$ [cd A$^{-1}$] | $PE_{max}$ [lm W$^{-1}$] | EQE [%] at max/100/1000 cd m$^{-2}$ |
|---|---|---|---|---|---|---|
| 10 wt% 32clCBP: DPEPO | 464 | 3.3 | 1000 | 29.1 | 27.7 | 16.0/12.2/2.7 |
| 20 wt% 32clCBP: DPEPO | 478 | 3 | 3350 | 35.5 | 34.3 | 16.3/15.4/9.9 |
| 30 wt% 32clCBP: DPEPO | 480 | 2.9 | 6640 | 33.6 | 36.4 | 14.2/13.0/9.7 |
| 10 wt% 32clCXT: DPEPO | 481 | 3.2 | 2600 | 44.9 | 43.4 | 20.6/18.0/12.0 |
| 20 wt% 32clCXT: DPEPO | 484 | 2.9 | 9360 | 50.8 | 54.3 | 21.2/20.6/16.8 |
| 30 wt% 32clCXT: DPEPO | 486 | 2.8 | 14 950 | 52.9 | 59.4 | 20.7/19.8/17.0 |
| 10 wt% 32PclCXT: DPEPO | 498 | 3.0 | 10 900 | 79.9 | 79.2 | 27.3/25.1/20.8 |
| 20 wt% 32PclCXT: DPEPO | 500 | 2.8 | 22 040 | 88.3 | 85.3 | 29.9/27.8/23.5 |
| 30 wt% 32PclCXT: DPEPO | 503 | 2.8 | 27 220 | 82.5 | 92.5 | 28.1/26.3//22.8 |

and EQE$_{max}$ of 21.2%. Remarkably, the doped 32PclCXT device delivered the best EL performance, achieving a CE$_{max}$ of 88.3 cd A$^{-1}$, PE$_{max}$ of 85.3 lm W$^{-1}$, and EQE$_{max}$ of 29.9%, along with outstanding efficiency stability and low efficiency roll-off with an 18% efficiency drop at a high luminance of 1000 cd m$^{-2}$. These performances rank among the highest efficiencies reported for TADF-OLEDs with similar emission wavelengths (Fig. S29, S30 and Table S4, ESI†). These results highlight the potential of 32PclCXT to address the critical challenge of efficiency roll-off for blue TADF emitters. Furthermore, we conducted measurements of the operating lifetime of these devices under unencapsulated conditions in an air atmosphere. The estimated LT$_{50}$ values at an initial luminance of 100 cd m$^{-2}$ were 1.35 hours, 1.68 hours, and 4.05 hours for the 20 wt% doped devices of 32clCBP, 32clCXT, and 32PclCXT (Fig. S31†), respectively.

## Conclusions

In summary, we have successfully developed three efficient blue/sky-blue luminogens, 32clCBP, 32clCXT, and 32PclCXT, featuring a rigid π-extended donor (5,12-dihydro-12-phenyl-indolo[3,2-a]carbazole) paired with various acceptors. These compounds, which can be synthesized through a straightforward one-step process, exhibit impressive thermal and morphological stability, making them ideal for large-scale production. Moreover, they exhibit AIE and TADF characteristics with small $\Delta E_{ST}$ values, faster RISC processes and higher PLQYs. Remarkably, the doped film of 32PclCXT achieves a PLQY of 99% and a short delayed lifetime of 1.4 µs. The corresponding device showcases outstanding electroluminescence performance, reaching an EQE$_{max}$ of 29.9% and a minimal efficiency roll-off of 18% at 1000 cd m$^{-2}$. These findings highlight the significant potential of indolocarbazole derivatives in achieving efficient blue OLED emitters and devices.

## Data availability

The data supporting this article have been included as part of the ESI.†

## Author contributions

Hui Dai: writing – original draft, methodology, investigation, data curation, conceptualization. Yaohui Liang: methodology,

investigation. Xiang Long: software, methodology. Tianyi Tang: investigation. Haozhi Xie: investigation. Zhiwei Ma: methodology. Gaoyu Li: methodology. Zhan Yang: writing – review & editing, supervision. Juan Zhao: writing – review & editing, supervision, funding acquisition. Zhenguo Chi: writing – review & editing, supervision, funding acquisition.

## Conflicts of interest

There are no conflicts to declare.

## Acknowledgements

## Notes and references

1 H. Uoyama, K. Goushi, K. Shizu, H. Nomura and C. Adachi, *Nature*, 2012, **492**, 234–238.
2 S.-G. Ihn, D. Jeong, E. S. Kwon, S. Kim, Y. S. Chung, M. Sim, J. Chwae, Y. Koishikawa, S. O. Jeon, J. S. Kim, J. Kim, S. Nam, I. Kim, S. Park, D. S. Kim, H. Choi and S. Kim, *Adv. Sci.*, 2022, **9**, 2102141.
3 M. Du, M. Mai, D. Zhang, L. Duan and Y. Zhang, *Chem. Sci.*, 2024, **15**, 3148–3154.
4 L. Yuan, J.-W. Xu, Z.-P. Yan, Y.-F. Yang, D. Mao, J.-J. Hu, H.-X. Ni, C.-H. Li, J.-L. Zuo and Y.-X. Zheng, *Angew. Chem., Int. Ed.*, 2024, **63**, e202407277.
5 X. Hong, D. Zhang, C. Yin, Q. Wang, Y. Zhang, T. Huang, J. Wei, X. Zeng, G. Meng, X. Wang, G. Li, D. Yang, D. Ma and L. Duan, *Chem*, 2022, **8**, 1705–1719.
6 Y. Wang, T. Yang, S. Dong, S. Zhao, W. Dong, H. Xu, X. Wang, Y. Miao and H. Wang, *ACS Mater. Lett.*, 2024, **6**, 1020–1028.
7 J. Wang, Y. Yang, C. Jiang, M. He, C. Yao and J. Zhang, *J. Mater. Chem. C*, 2022, **10**, 3163–3171.
8 J. Li, Y. Xia, G. Li, M. Chen, J. Zhou, W. Yan, B. Zhao, K. Guo and H. Wang, *Chem. Eng. J.*, 2023, **470**, 143966.
9 Z. Yang, Z. Mao, C. Xu, X. Chen, J. Zhao, Z. Yang, Y. Zhang, W. Wu, S. Jiao, Y. Liu, M. P. Aldred and Z. Chi, *Chem. Sci.*, 2019, **10**, 8129–8134.

10 H. Wang, J.-X. Chen, L. Zhou, X. Zhang, J. Yu, K. Wang and X.-H. Zhang, *Mater. Horiz.*, 2023, **10**, 2997–3004.

11 Z.-Q. Feng, Y.-J. Yu, Z.-Y. Song, M. Song, P. Zuo, Z.-Q. Jiang, D.-Y. Zhou and L.-S. Liao, *Adv. Funct. Mater.*, 2024, 2403831.

12 Q.-Y. Meng, R. Wang, Y.-L. Wang, X.-W. Guo, Y.-Q. Liu, X.-L. Wen, C.-Y. Yao and J. Qiao, *Nat. Commun.*, 2023, **14**, 3927.

13 C. Wu, C. Shi, Y. Zheng, J. Zhang, Y. Wang, N. Sun, Q. Wang and Z.-H. Lu, *Chem. Eng. J.*, 2022, **431**, 133249.

14 J. Fang, Z. Liu, J. Li, N. Zhuang, D. Yang, D. Ma, B. Z. Tang and Z. Zhao, *Adv. Opt. Mater.*, 2023, **11**, 2300835.

15 M. Mamada, H. Katagiri, C.-Y. Chan, Y.-T. Lee, K. Goushi, H. Nakanotani, T. Hatakeyama and C. Adachi, *Adv. Funct. Mater.*, 2022, **32**, 2204352.

16 Y. Wang, Z. Ma, J. Pu, D. Guo, G. Li, Z. Chen, S.-J. Su, H. Deng, J. Zhao and Z. Chi, *Aggregate*, 2024, **5**, e585.

17 J. Xue, J. Xu, Q. Liang, Y. Dai, R. Wang, Y. Yi and J. Qiao, *Adv. Funct. Mater.*, 2023, **33**, 2301312.

18 Z. Liu, J. Chen, L. Chen, H. Liu, D. Yang, D. Ma, B. Z. Tang and Z. Zhao, *Small*, 2023, **20**, 2305589.

19 J. Wang, Y. Yang, F. Gu, X. Zhai, C. Yao, J. Zhang, C. Jiang and X. Xi, *ACS Appl. Mater. Interfaces*, 2023, **15**, 59643–59654.

20 D. Karthik, S. Y. Lee, D. H. Ahn, H. Lee, J. Y. Lee, J. H. Kwon and J. H. Park, *Org. Electron.*, 2019, **74**, 282–289.

21 J. Wang, Y. Niu, Y. Yang, H. Peng, J. Zhang and C. Yao, *Mater. Today Chem.*, 2024, **40**, 102239.

22 J. Chen, Z. Liu, L. Chen, P. Zou, B. Z. Tang and Z. Zhao, *Small*, 2023, **20**, 2306800.

23 Y. Fu, H. Liu, B. Z. Tang and Z. Zhao, *Nat. Commun.*, 2023, **14**, 2019.

24 Y. Fu, H. Liu, B. Z. Tang and Z. Zhao, *Adv. Funct. Mater.*, 2024, **34**, 2401434.

25 G. Li, J. Pu, Z. Yang, H. Deng, Y. Liu, Z. Mao, J. Zhao, S.-J. Su and Z. Chi, *Aggregate*, 2023, **4**, e382.

26 X. Ge, G. Li, D. Guo, Z. Yang, Z. Mao, J. Zhao and Z. Chi, *Adv. Opt. Mater.*, 2024, **12**, 2302535.